NUCL SCI TECH (2020) 31:109
https://doi.org/10.1007/s41365-020-00821-7

Effective (kinetic freeze-out) temperature, transverse flow velocity, and kinetic freeze-out volume in high energy collisions

Muhammad Waqas[1,2,3] · Fu-Hu Liu[1,2] · Li-Li Li[1,2] · Haidar Mas'ud Alfanda[4]

Received: 2 August 2020 / Revised: 25 August 2020 / Accepted: 17 September 2020 / Published online: 7 November 2020

Abstract The transverse momentum spectra of different types of particles produced in central and peripheral gold–gold (Au–Au) and inelastic proton–proton (*pp*) collisions at the Relativistic Heavy Ion Collider, as well as in central and peripheral lead-lead (Pb–Pb) and *pp* collisions at the Large Hadron Collider, are analyzed by the multi-component standard (Boltzmann–Gibbs, Fermi–Dirac, and Bose–Einstein) distributions. The obtained results from the standard distribution give an approximate agreement with the measured experimental data by the STAR, PHENIX, and ALICE Collaborations. The behavior of the effective (kinetic freeze-out) temperature, transverse flow velocity, and kinetic freeze-out volume for particles with different masses is obtained, which observes the early kinetic freeze-out of heavier particles as compared to the lighter particles. The parameters of emissions of different particles are observed to be different, which reveals a direct signature of the mass-dependent differential kinetic freeze-out. It is also observed that the peripheral nucleus–nucleus (*AA*) and *pp* collisions at the same center-of-mass energy per nucleon pair are in good agreement in terms of the extracted parameters.

Keywords Transverse momentum spectra · Effective temperature · Kinetic freeze-out temperature · Transverse flow velocity · Kinetic freeze-out volume

This work was supported by the National Natural Science Foundation of China (Nos. 11575103 and 11947418), the Chinese Government Scholarship (China Scholarship Council), the Scientific and Technological Innovation Programs of Higher Education Institutions in Shanxi (STIP) (No. 201802017), the Shanxi Provincial Natural Science Foundation (No. 201901D111043), and the Fund for Shanxi "1331 Project" Key Subjects Construction.

✉ Fu-Hu Liu
fuhuliu@163.com; fuhuliu@sxu.edu.cn

1 Institute of Theoretical Physics and State Key Laboratory of Quantum Optics and Quantum Optics Devices, Shanxi University, Taiyuan 030006, China

2 Collaborative Innovation Center of Extreme Optics, Shanxi University, Taiyuan 030006, China

3 School of Nuclear Science and Technology, University of Chinese Academy of Sciences, Beijing 100049, China

4 Key Laboratory of Quark and Lepton Physics (MOE) and Institute of Particle Physics, Central China Normal University, Wuhan 430079, China

1 Introduction

A hot and dense fireball is assumed to form for a brief period of time ($\sim$ a few fm/c) over an extended region after the initial collisions, which undergoes a collective expansion that leads to the change in the temperature and volume or density of the system. Three types of temperatures, namely the initial temperature, chemical freeze-out temperature, and kinetic freeze-out temperature, can be found in the literature, which describe the excitation degrees of an interacting system at the stages of initial collisions, chemical freeze-out, and kinetic freeze-out, respectively [1–7]. There is another type of temperature, namely the effective temperature, which is not a real temperature and it describes the sum of excitation degrees of the interacting system and the effect of transverse flow at the stage of kinetic freeze-out.

In principle, the initial stage of collisions happens earlier than other stages such as the chemical and kinetic freeze-out stages. Naturally, the initial temperature is the highest, and the kinetic freeze-out temperature is the lowest among the three real temperatures, while the chemical freeze-out temperature is in between the initial and kinetic freeze-out temperatures. The collision system does not get rid of the simultaneity for chemical and kinetic freeze-outs, which results in the chemical and kinetic freeze-out temperatures to be the same. The effective temperature is often larger than the kinetic freeze-out temperature but is equal to the kinetic freeze-out temperature in case of zero transverse flow velocity.

To understand the given nature of the nuclear force and to break the system into massive fragments [8, 9], it is a good way to make the nucleons interact in nucleus–nucleus (*AA*) collisions at intermediate and high energies. Such a process provokes a liquid–gas type phase transition as a large number of nucleons and other light nuclei are emitted. In *AA* collisions at higher energies, a phase transition from hadronic matter to quark–gluon plasma (QGP) is expected to occur. The volume occupied by the source of such ejectiles, where the mutual nuclear interactions become negligible (they only feel the Coulombic repulsive force and not the attractive force), is said to be kinetic freeze-out volume and it has been introduced in various statistical and thermodynamic models [10, 11]. Similar to the kinetic freeze-out temperature, the kinetic freeze-out volume also gives the information of the coexistence of phase transition. This is one of the major factors, which are important in the extraction of vital observables such as multiplicity, micro-canonical heat capacity, and its negative branch or shape of caloric curves under the external constraints [12–16].

It is conceivable that the temperature (volume) of the interacting system decreases (increases) from the initial state to the final kinetic freeze-out stage. During the evolution process, the transverse flow velocity is present due to the expansion of the interacting system. The study of the dependence of effective (kinetic freeze-out) temperature, transverse flow velocity, and kinetic freeze-out volume on the collision energy, event centrality, system size, and particle rapidity is very significant. We are very interested in the aforementioned quantities in central and peripheral *AA* and (inelastic) proton–proton (*pp*) collisions at the Relativistic Heavy Ion Collider (RHIC) and the Large Hadron Collider (LHC) over a wide enough energy range in which QGP is expected to form.

Here, we study the dependence of effective (kinetic freeze-out) temperature, transverse flow velocity, and kinetic freeze-out volume in central and peripheral gold–gold (Au–Au) and lead–lead (Pb–Pb) collisions at the RHIC and LHC energies and compare their peripheral collisions with *pp* collisions of the same center-of-mass energy per nucleon pair $\sqrt{s_{\mathrm{NN}}}$ (or the center-of-mass energy $\sqrt{s}$ for *pp* collisions). Only 62.4 GeV at the RHIC and 5.02 TeV at the LHC are considered as examples. We present the approach of effective temperature and kinetic freeze-out volume from the transverse momentum spectra of the identified particles produced in the mentioned *AA* and *pp* collisions. The kinetic freeze-out temperature and transverse flow velocity are then obtained from particular linear relations.

The remainder of this manuscript is structured as follows. The formalism and method are described in Sect. 2. The results and discussion are given in Sect. 3. In Sect. 4, we summarize our main observations and conclusions.

2 Method and formalism

Generally, two main processes of particle production are under consideration, which includes the soft and hard excitation processes. The soft excitation process corresponds to strong interactions among multiple partons, while the hard excitation process corresponds to a more violent collision between two head-on partons. The soft excitation process has numerous choices of formalisms, including but not limited to the Hagedorn thermal model (statistical-bootstrap model) [17], the (multi-)standard distribution [18], the Tsallis and related distributions with various formalisms [19], the blast-wave model with Tsallis statistics [20], the blast-wave model with Boltzmann statistics [21–25], and other thermodynamics-related models [26–29]. The hard excitation process has very limited choices of formalisms and can be described by the perturbative quantum chromodynamics (pQCD) [30–32].

The experimental data of the transverse momentum (p_{T}) spectrum of the particles are fitted using the standard distribution, which is the combination of Boltzmann–Gibbs, Fermi–Dirac, and Bose–Einstein distributions corresponding to the factor $S = 0$, $+1$, and -1, respectively. The standard distribution at the mid-rapidity can be demonstrated as [18]

$$f_S(p_{\mathrm{T}}) = \frac{1}{N}\frac{\mathrm{d}N}{\mathrm{d}p_{\mathrm{T}}} = \frac{1}{N}\frac{gV'}{(2\pi)^2}p_{\mathrm{T}}\sqrt{p_{\mathrm{T}}^2+m_0^2} \times\left[\exp\left(\frac{\sqrt{p_{\mathrm{T}}^2+m_0^2}}{T}\right)+S\right]^{-1}, \tag{1}$$

where the chemical potential is neglected. Here, N is the experimental number of considered particles, T is the fitted effective temperature, V' is the fitted kinetic freeze-out volume (i.e., the interaction volume) of the emission source at the kinetic freeze-out stage, $g = 3$ (or 2) is the degeneracy factor for pions and kaons (or protons), and m_0 is the rest mass of the considered particle. As a probability density function, the integral of Eq. (1) is naturally normalized to 1, i.e., we have $\int_0^{p_{\mathrm{T}\max}} f_S(p_\mathrm{T})\mathrm{d}p_\mathrm{T}=1$, where $p_{\mathrm{T}\max}$ denotes the maximum p_T. At very high energy, the influence of $S=+1$ and -1 can be neglected. Only the Boltzmann–Gibbs distribution is sufficient to describe the spectra at the RHIC and LHC.

Considering the experimental rapidity range $[y_{\min}, y_{\max}]$ around mid-rapidity, Eq. (1) takes the form

$$f_S(p_\mathrm{T})=\frac{1}{N}\frac{gV'}{(2\pi)^2}p_\mathrm{T}\int_{y_{\min}}^{y_{\max}}\left(\sqrt{p_\mathrm{T}^2+m_0^2}\cosh y-\mu\right)\times\left[\exp\left(\frac{\sqrt{p_\mathrm{T}^2+m_0^2}\cosh y-\mu}{T}\right)+S\right]^{-1}\mathrm{d}y, \tag{2}$$

where the chemical potential μ is particle dependent, which we have studied recently [33]. In high energy collisions, μ_j ($j=\pi$, K, and p) are less than several MeV, which slightly affects V' compared with that for $\mu_j=0$. Then, we may regard $\mu\approx 0$ in Eq. (2) at high energies considered in the present study. In Eqs. (1) and (2), only T and V' are the free parameters.

Usually, we have to use the two-component standard distribution because single-component standard distribution is not enough for the simultaneous description of very low- ($0\sim 0.2-0.3$ GeV/c) and low-p_T (0.2–$0.3\sim 2-3$ GeV/c or slightly more) regions, which are contributed by the resonance decays and other soft excitation processes, respectively. More than two or multi-component standard distributions can also be used in some cases. We have the simplified multi-component (l-component) standard distribution to be

$$f_S(p_\mathrm{T})=\sum_{i=1}^{l}k_i\frac{1}{N_i}\frac{gV_i'}{(2\pi)^2}p_\mathrm{T}\sqrt{p_\mathrm{T}^2+m_0^2}\times\left[\exp\left(\frac{\sqrt{p_\mathrm{T}^2+m_0^2}}{T_i}\right)+S\right]^{-1}, \tag{3}$$

where N_i and k_i denote, respectively, the particle number and fraction contributed by the ith component, and T_i and V_i' denote, respectively, the effective temperature and kinetic freeze-out volume corresponding to the ith component.

More accurate form of l-component standard distribution can be written as,

$$f_S(p_\mathrm{T})=\sum_{i=1}^{l}k_i\frac{1}{N_i}\frac{gV_i'}{(2\pi)^2}p_\mathrm{T}\times\int_{y_{\min}}^{y_{\max}}\left(\sqrt{p_\mathrm{T}^2+m_0^2}\cosh y-\mu\right)\times\left[\exp\left(\frac{\sqrt{p_\mathrm{T}^2+m_0^2}\cosh y-\mu}{T_i}\right)+S\right]^{-1}\mathrm{d}y. \tag{4}$$

In Eqs. (3) and (4), only T_i, V_i', and k_i ($i\le l-1$) are free parameters. Generally, $l=2$ or 3 is enough for describing the spectra in a not too wide p_T range.

Equations (1) or (2) and (3) or (4) can be used for the description of p_T spectra and for the extraction of effective temperature and kinetic freeze-out volume in very low- and low-p_T regions. The high-p_T ($>3-4$ GeV/c) region contributed by the hard excitation process has to be fitted by the Hagedorn function [17], which is an inverse power law function, given by

$$f_H(p_\mathrm{T})=\frac{1}{N}\frac{\mathrm{d}N}{\mathrm{d}p_\mathrm{T}}=Ap_\mathrm{T}\left(1+\frac{p_\mathrm{T}}{p_0}\right)^{-n}. \tag{5}$$

It results from the pQCD [30–32], where A is the normalization constant, which depends on the free parameters p_0 and n, and results in $\int_0^{p_{\mathrm{T}\max}} f_H(p_\mathrm{T})dp_\mathrm{T}=1$.

While considering the contributions of both the soft and hard excitation processes, we used the superposition in principle

$$f_0(p_\mathrm{T})=kf_S(p_\mathrm{T})+(1-k)f_H(p_\mathrm{T}), \tag{6}$$

where k is the contribution ratio of the soft process and gives a natural result in $\int_0^{p_{\mathrm{T}\max}} f_0(p_\mathrm{T})\mathrm{d}p_\mathrm{T}=1$. In Eq. (6), the contribution of the soft process is from 0 to $\sim 2-3$ GeV/c, or even up to $\sim 3-5$ GeV/c at very high energy, and the hard component contributes to the whole p_T range. There is some mixing between the contributions of the two processes in the low-p_T region.

According to the Hagedorn model [17], the contributions of the two processes can be separated completely. One has another superposition

$$f_0(p_\mathrm{T})=A_1\theta(p_1-p_\mathrm{T})f_S(p_\mathrm{T})+A_2\theta(p_\mathrm{T}-p_1)f_H(p_\mathrm{T}), \tag{7}$$

where $\theta(x)$ is the usual step function and A_1 and A_2 are the normalization constants, which make $A_1f_S(p_1)=A_2f_H(p_1)$. Equation (7) gives the contribution of soft process from 0 to p_1, while the hard component contributes from p_1 up to the maximum.

In the aforementioned two-component functions [Eqs. (6) and (7)], each component ($f_S(p_\mathrm{T})$ and $f_H(p_\mathrm{T})$) is a traditional distribution. The first component ($f_S(p_\mathrm{T})$) is one of the Boltzmann–Gibbs, Fermi–Dirac, and Bose–Einstein distributions if we use a given S, such as $S=0$, $+1$, or -1. The second component ($f_H(p_\mathrm{T})$) is the Tsallis-like distribution [19] if we let $n=1/(q-1)$ and $p_0=nT_\mathrm{T}$, where q is the entropy index and T_T is the Tsallis temperature.

We will use only the first component in Eq. (7) due to the reason that we are not studying a wide p_T range in the present work. In the case of neglecting the contribution of the hard component in the low-p_T region in Eq. (6), the first component in Eq. (6) gives the same result as that of the first component in Eq. (7). Equation (4) with $l=2$, which is the two-component standard distribution, is used in the present work. In addition, considering the treatment of normalization, the real fitted kinetic freeze-out volume should be $V_1 = N_1 V_1'/k_1$ and $V_2 = N_2 V_2'/(1-k_1)$, which will be simply used in the following section.

It should be noted that the value of l in the l-component standard distribution has some influences on the free parameters and then on the derived parameters. Generally, $l=1$ is not enough to fit the particle spectra. For $l=2$, the influence of the second component is obvious since the contribution of the first component is not sufficient to fit the particle spectra. For $l=3$, the influence of the third component is rather small because the main contribution is from the first two components, and the contribution of the third component can be neglected.

3 Results and discussion

3.1 Comparison with the data

Figure 1a, b demonstrates the transverse momentum spectra, $(1/2\pi p_T)d^2N/dp_Tdy$, of the negatively charged particles π^-, K^-, and $\bar{p}$ produced in (a) central (0–10%), and (b) peripheral (40–80%) Au–Au collisions at $\sqrt{s_{NN}} =$ 62.4 GeV. The circles, triangles, and squares represent the experimental data measured in the mid-rapidity range $-0.5 < y < 0$ at the RHIC by the STAR Collaboration [34]. The curves represent fitting results by Eq. (4) with $l=2$. Following each panel, the results of Data/Fit are presented. The values of the related parameters (T_1, T_2, V_1, V_2, k_1, and N_0) along with the χ^2 and the number of degrees of freedom (ndof) are given in Table 1. It can be seen that the two-component standard distribution fits approximately the experimental data measured at mid-rapidity in Au–Au collisions at the RHIC.

To see the contributions of the two components in Eq. (4) with $l=2$, as examples, Fig. 1c, d shows the contributions of the first and second components by the dashed and dotted curves, respectively, and the total contribution is given by the solid curves. Only the results of π^- produced in (c) central (0–10%) and (d) peripheral (40–80%) Au–Au collisions at $\sqrt{s_{NN}} = 62.4$ GeV are presented. The circles represent the same data points as those in Fig. 1a, b. One can see that the first component contributes mainly to the very low- and low-p_T region, while the second component contributes to a wider region. There is a large overlap region of the two contributions.

The transverse momentum spectra, $(1/N_{ev})d^2N/dp_Tdy$, of π^-, K^-, and $\bar{p}$ produced in (a) central (0–5%), and (b) peripheral (80–90%) Pb–Pb collisions at $\sqrt{s_{NN}} = 5.02$ TeV are shown in Fig. 2, where N_{ev} on the vertical axis denotes the number of events. The experimental data of π^-, K^-, and $\bar{p}$ measured in the mid-rapidity range $|y| < 0.5$ at the LHC by the ALICE Collaboration [35, 36] are represented by circles, triangles, and squares, respectively. The curves are our results fitted by Eq. (4) with $l=2$. Following each panel, the results of Data/Fit are presented. The values of the related parameters along with the χ^2 and ndof are given in Table 1. One can see that the two-component standard distribution fits approximately the experimental data measured in the mid-rapidity range in Pb–Pb collisions at the LHC.

The fitting in Figs. 1 and 2 for peripheral collisions appears to be worse compared to central collisions. This is caused by a statistical fluctuation and the effect of a cold spectator in peripheral collisions. In the region of the cold spectator, particles are produced by multiple cascade scattering processes which are different from the thermalization processes of particle production in the region of the hot participants. In addition, our fits are done in all ranges of $p_T < 4.5$ GeV/c. However, as an alternative model, the blast-wave fit takes different cuts of p_T for the analysis of different particles (see for instance Ref. [2]). These different cuts affect the extraction of parameters, in particular for the analysis of the trends of particles, which is not an ideal treatment.

In the next fits, we used all ranges of $p_T < 4.5$ GeV/c. Figure 3a, b shows the transverse momentum spectra, $Ed^3\sigma/dp^3 = (1/2\pi p_T)d^2\sigma/dp_Tdy$, of π^-, K^-, and $\bar{p}$ produced in pp collisions at $\sqrt{s} = 62.4$ GeV and 5.02 TeV, respectively. E and σ on the vertical axis denote the energy and cross section, respectively. The symbols represent the experimental data measured in the mid-pseudorapidity range $|\eta| < 0.35$ by the PHENIX Collaboration [37] and in the mid-rapidity range $|y| < 0.5$ by the ALICE Collaborations [35, 36]. The curves represent our results, fitted by Eq. (4) with $l=2$. Following each panel, the results of Data/Fit are presented. The values of the related parameters (N_0 in Figs. 1 and 2 are replaced by σ_0 in Fig. 3) along with χ^2 and ndof are given in Table 1. One can see that the two-component standard distribution fits approximately the experimental data measured at mid-(pseudo)rapidity in pp collisions at the RHIC and LHC.

We would like to point out that the vertical axes of Figs. 1, 2 and 3 are not the probability density function. We cannot fit them with Eq. (4) with $l=2$. Hence, we have done a conversion during our fitting. For Fig. 1, we have used the relation $(1/2\pi p_T)(d^2N/dp_Tdy) = (1/2\pi p_T)N_0 f_S(p_T)/dy$ for the conversion, where N_0 is the normalization constant in terms of particle number. For Fig. 2, we have used the relation $d^2N/dp_Tdy = N_0 f_S(p_T)/dy$ for the conversion, where N_{ev} on the vertical axis is neglected because d^2N/dp_Tdy is directly regarded as

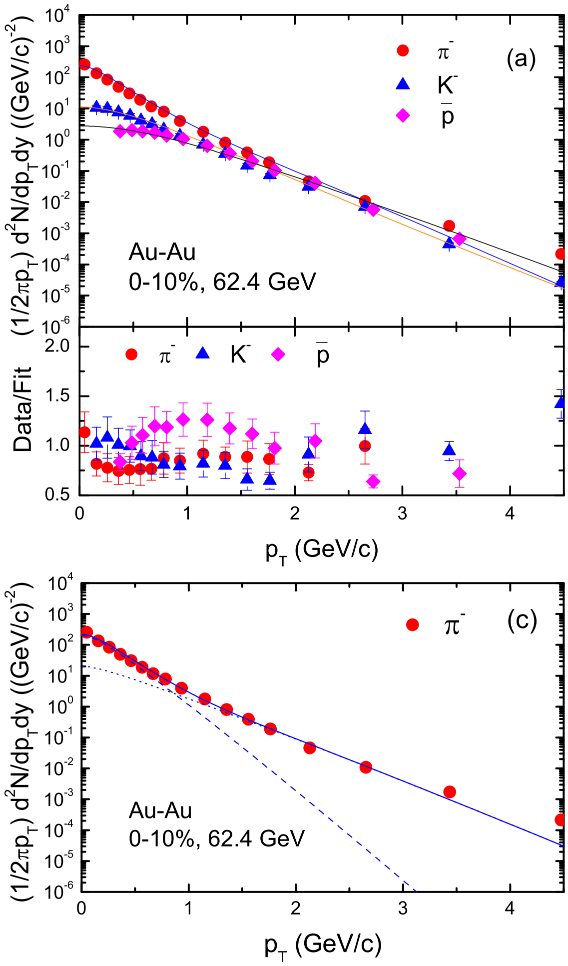

Fig. 1 (Color online) **a**, **b** Transverse momentum spectra of π^-, K^-, and $\bar{p}$ produced in **a** central (0–10%) and **b** peripheral (40–80%) Au–Au collisions at $\sqrt{s_{NN}} = 62.4$ GeV. The symbols represent the experimental data measured in the range $-0.5 < y < 0$ at the RHIC by the STAR Collaboration [34]. The curves represent the fitting results by Eq. (4) with $l = 2$. Following each panel, the results of Data/Fit are presented. **c**, **d** As examples, panels **c** and **d** show the contributions of the first and the second components in Eq. (4) with $l = 2$ by the dashed and dotted curves, respectively, and the total contribution is given by the solid curves. The circles in panels **c** and **d** represent the same data as those in panels **a** and **b**, respectively

the result per event. For Fig. 3, we have used the relation $Ed^3\sigma/dp^3 = (1/2\pi p_T)(d^2\sigma/dp_T dy) = (1/2\pi p_T)\sigma_0 f_S(p_T)/dy$ in the conversion, where σ_0 is the normalization constant in terms of the cross section.

From Figs. 1, 2 and 3 and Table 1, it can be seen that the fitting quality is not great in some cases. It should be pointed out that the model used in these fittings is for soft processes but is used for analyzing p_T spectra up to 4.5 GeV/c. The high values of p_T analyzed in this study contain hard processes which could be responsible for the bad fitting as indicated by χ^2 in Table 1 and also in the ratio of data to the fitting of Figs. 1, 2 and 3. Then, it may seem necessary to attempt fitting by taking into account the function part corresponding to the hard process. However, the hard process is not necessary for extracting the parameters of the soft process. Although the fittings will be better if we also consider the contribution of the hard process, it is not useful for extracting the parameters considered in the present work. Therefore, we did not consider the contribution of the hard process.

3.2 Discussion on the parameters

Considering the contributions of the two components, the effective temperature averaged over the two components is $T = k_1T_1 + k_2T_2$ and the kinetic freeze-out volume by adding the two components is $V = V_1 + V_2$. Further, the normalization constants contributed by the first and the second components are k_1N_0 and k_2N_0, respectively.

For convenience, we introduced the average p_T ($\langle p_T \rangle$) and average moving mass ($\overline{m}$, i.e., average energy in the source rest frame) here. Considering Eq. (4) only, we have

Table 1 Values of parameters (T_1, T_2, V_1, V_2, k_1, and N_0 (for Figs. 1 and 2) or σ_0 [for Fig. 3)], χ^2, and the ndof corresponding to the solid curves in Figs. 1, 2 and 3

Collisions	Centrality	Particle	T_1 (GeV)	T_2 (GeV)	V_1 (fm^3)	V_2 (fm^3)	k_1	N_0 [σ_0 (mb)]	χ^2	ndof
Figure 1	0–10%	π^-	0.141 ± 0.008	0.285 ± 0.007	185 ± 13	3330 ± 270	0.88 ± 0.07	0.080 ± 0.004	43	14
Au–Au		K^-	0.199 ± 0.009	0.316 ± 0.007	19 ± 1	2034 ± 162	0.85 ± 0.11	0.010 ± 0.003	174	13
62.4 GeV		$\bar{p}$	0.280 ± 0.012	0.340 ± 0.004	22 ± 3	1053 ± 100	0.92 ± 0.10	0.020 ± 0.004	56	11
	40–80%	π^-	0.070 ± 0.006	0.250 ± 0.006	32 ± 5	127 ± 14	0.70 ± 0.07	0.025 ± 0.050	94	14
		K^-	0.239 ± 0.008	0.260 ± 0.004	2.3 ± 0.3	118 ± 18	0.89 ± 0.09	0.005 ± 0.001	40	13
		$\bar{p}$	0.201 ± 0.007	0.302 ± 0.005	3.0 ± 0.2	69 ± 8	0.89 ± 0.11	0.009 ± 0.001	7	11
Figure 2	0–5%	π^-	0.267 ± 0.013	0.624 ± 0.005	8943 ± 655	4341 ± 200	0.93 ± 0.12	1.770 ± 0.300	425	33
Pb–Pb		K^-	0.355 ± 0.014	0.465 ± 0.006	1820 ± 250	5555 ± 300	0.94 ± 0.12	0.300 ± 0.040	776	32
5.02 TeV		$\bar{p}$	0.459 ± 0.014	0.512 ± 0.006	381 ± 30	5476 ± 240	0.94 ± 0.10	0.325 ± 0.040	748	30
	80–90%	π^-	0.200 ± 0.009	0.407 ± 0.004	154 ± 8	246 ± 50	0.70 ± 0.09	0.060 ± 0.003	658	33
		K^-	0.198 ± 0.016	0.420 ± 0.005	17 ± 2	264 ± 45	0.90 ± 0.11	0.020 ± 0.003	90	32
		$\bar{p}$	0.302 ± 0.018	0.400 ± 0.006	4.4 ± 0.5	330 ± 56	0.92 ± 0.13	0.008 ± 0.001	296	29
Figure 3a	–	π^-	0.182 ± 0.006	0.275 ± 0.005	65 ± 8	22 ± 4	0.68 ± 0.12	0.350 ± 0.060	54	23
pp		K^-	0.160 ± 0.007	0.255 ± 0.006	5.0 ± 0.4	77 ± 10	0.88 ± 0.15	0.007 ± 0.001	4	13
62.4 GeV		$\bar{p}$	0.235 ± 0.008	0.260 ± 0.006	1.6 ± 0.1	50 ± 6	0.95 ± 0.10	0.008 ± 0.001	126	24
Figure 3b	–	π^-	0.090 ± 0.008	0.370 ± 0.005	16 ± 2	101 ± 13	0.64 ± 0.11	0.016 ± 0.003	945	33
pp		K^-	0.850 ± 0.013	0.370 ± 0.004	0.80 ± 0.04	97 ± 12	0.87 ± 0.11	0.007 ± 0.001	666	31
5.02 TeV		$\bar{p}$	0.539 ± 0.010	0.391 ± 0.005	1.1 ± 0.1	77 ± 12	0.90 ± 0.13	0.003 ± 0.001	496	29

From the table, we have $k_2 = 1 - k_1$, $T = k_1T_1 + k_2T_2$, and $V = V_1 + V_2$. The normalization constants contributed by the first and the second components are k_1N_0 (or $k_1\sigma_0$) and k_2N_0 (or $k_2\sigma_0$), respectively

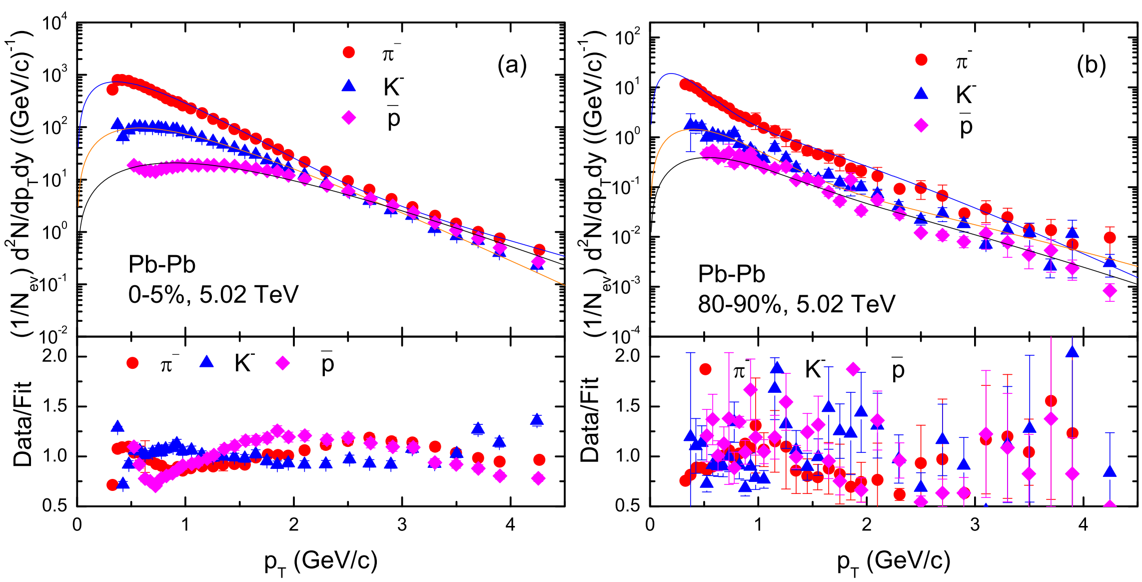

Fig. 2 (Color online) Transverse momentum spectra of π^-, K^-, and $\bar{p}$ produced in **a** central (0–5%) and **b** peripheral (80–90%) Pb–Pb collisions at $\sqrt{s_{\mathrm{NN}}} = 5.02$ TeV. The symbols represent the experimental data measured at $|y| < 0.5$ at the LHC by the ALICE Collaboration [35, 36]. The curves represent fitting by Eq. (4) with $l = 2$. Following each panel, the results of Data/Fit are presented

$$\langle p_{\mathrm{T}} \rangle = \int_0^{p_{\mathrm{T\,max}}} p_{\mathrm{T}} f_S(p_{\mathrm{T}}) dp_{\mathrm{T}}. \tag{8}$$

To obtain $\overline{m}$, we can use the Monte Carlo method. Let R_1 and R_2 denote random numbers distributed evenly in [0, 1].

A concrete value of p_{T} that satisfies Eq. (4) can be obtained by

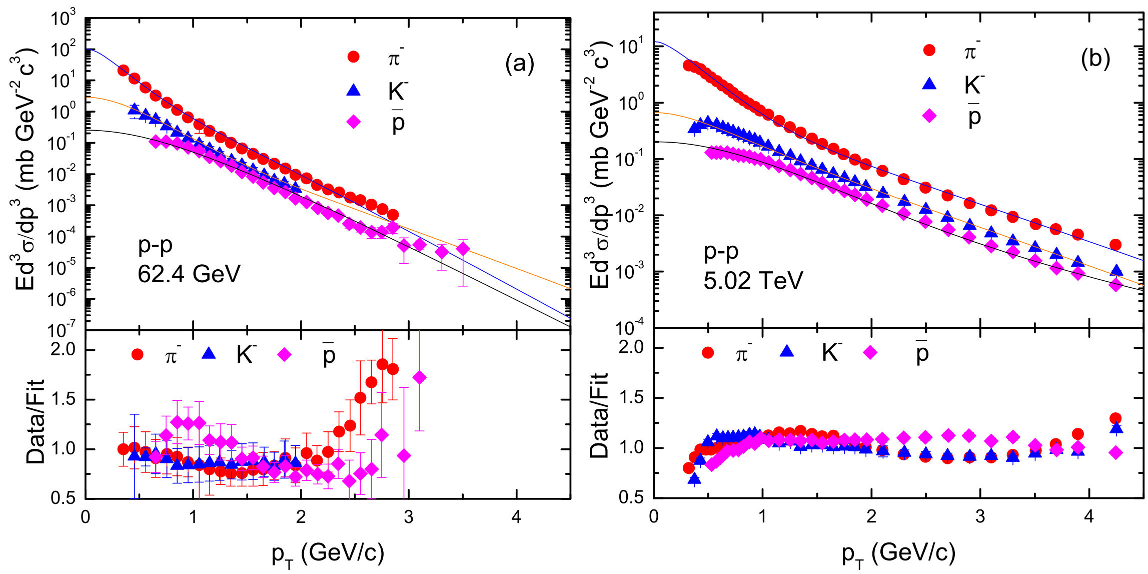

Fig. 3 (Color online) Transverse momentum spectra of π^-, K^-, and $\bar{p}$ produced in *pp* collisions at **a** $\sqrt{s} = 62.4$ GeV and **b** $\sqrt{s} = 5.02$ TeV. The symbols represent the experimental data measured at $|\eta| < 0.35$ by the PHENIX Collaboration [37] and at $|y| < 0.5$ by the ALICE Collaborations [35, 36]. The curves represent our results, fitted by Eq. (4) with $l = 2$. Following each panel, the results of Data/Fit are presented

$$\int_0^{p_\mathrm{T}} f_S(p'_\mathrm{T})\mathrm{d}p'_\mathrm{T} < R_1 < \int_0^{p_\mathrm{T}+\delta p_\mathrm{T}} f_S(p'_\mathrm{T})\mathrm{d}p'_\mathrm{T}, \tag{9}$$

where δp_T denotes a small shift relative to p_T. In the source rest frame and under the assumption of isotropic emission, the emission angle θ of the considered particle obeys

$$f_\theta(\theta) = \frac{1}{2}\sin\theta. \tag{10}$$

which results in

$$\theta = 2\arcsin\left(\sqrt{R_2}\right) \tag{11}$$

in the Monte Carlo method [38]. Then,

$$m = \sqrt{(p_\mathrm{T}/\sin\theta)^2 + m_0^2}. \tag{12}$$

After repeating the calculation many times, we can obtain $\overline{m}$.

To study the change in the trends of parameters with the particle mass, Fig. 4a, b shows the dependences of T on m_0 for productions of negative charged particles in central and peripheral (a) Au–Au collisions at 62.4 GeV and (b) Pb–Pb collisions at 5.02 TeV, while *pp* collisions at (a) 62.4 GeV and (b) 5.02 TeV are also studied and compared to peripheral *AA* collisions of the same energy (per nucleon pair). Correspondingly, Fig. 4c, d shows the dependences of $\langle p_\mathrm{T}\rangle$ on $\overline{m}$ for the mentioned particles in the considered collisions. The filled, empty, and half-filled symbols represent central *AA*, peripheral *AA*, and *pp* collisions, respectively. The lines represent linear fittings of the relations. The related linear fitting parameters are listed in Table 2, though some of them are not good fitting due to very large χ^2. The intercept in the linear relation between T and m_0 is regarded as the kinetic freeze-out temperature T_0, and the slope in the linear relation between $\langle p_\mathrm{T}\rangle$ and $\overline{m}$ is regarded as the transverse flow velocity β_T. That is, $T = am_0 + T_0$ [24, 39, 40] and $\langle p_\mathrm{T}\rangle = \beta_T\overline{m} + b$, where a and b are free parameters.

Note that the relation $T = am_0 + T_0$ [24, 39, 40] is used because the intercept should be the kinetic freeze-out temperature T_0 which corresponds to the emission of massless particles for which, there is no influence of the flow effect. The relation $\langle p_\mathrm{T}\rangle = \beta_\mathrm{T}\overline{m} + b$ was used in our previous works [22, 23, 41, 42] for the same dimensions of $\langle p_\mathrm{T}\rangle$ and $\beta_\mathrm{T}\overline{m}$. The interpretation of slope a in $T = am_0 + T_0$ and the intercept b in $\langle p_\mathrm{T}\rangle = \beta_\mathrm{T}\overline{m} + b$ is not clear to us. Possibly, am_0 reflects the effective temperature contributed by the flow effect and b reflects the average transverse momentum contributed by the thermal motion.

From Fig. 4 and Table 2, one can see that T (T_0 or β_T) is larger in the central *AA* collisions as compared to peripheral *AA* collisions, and peripheral *AA* collisions are comparable with the *pp* collisions at the same $\sqrt{s_\mathrm{NN}}$ ($\sqrt{s}$). The mass-dependent or differential kinetic freeze-out scenario for T is observed, as T increased with the increase in m_0. The present work confirms various mass-dependent or differential kinetic freeze-out scenarios [2, 3, 20, 43, 44]. Because T_0 (β_T) is obtained from the linear relation between T and m_0 ($\langle p_\mathrm{T}\rangle$ and $\overline{m}$), it seems that there is no

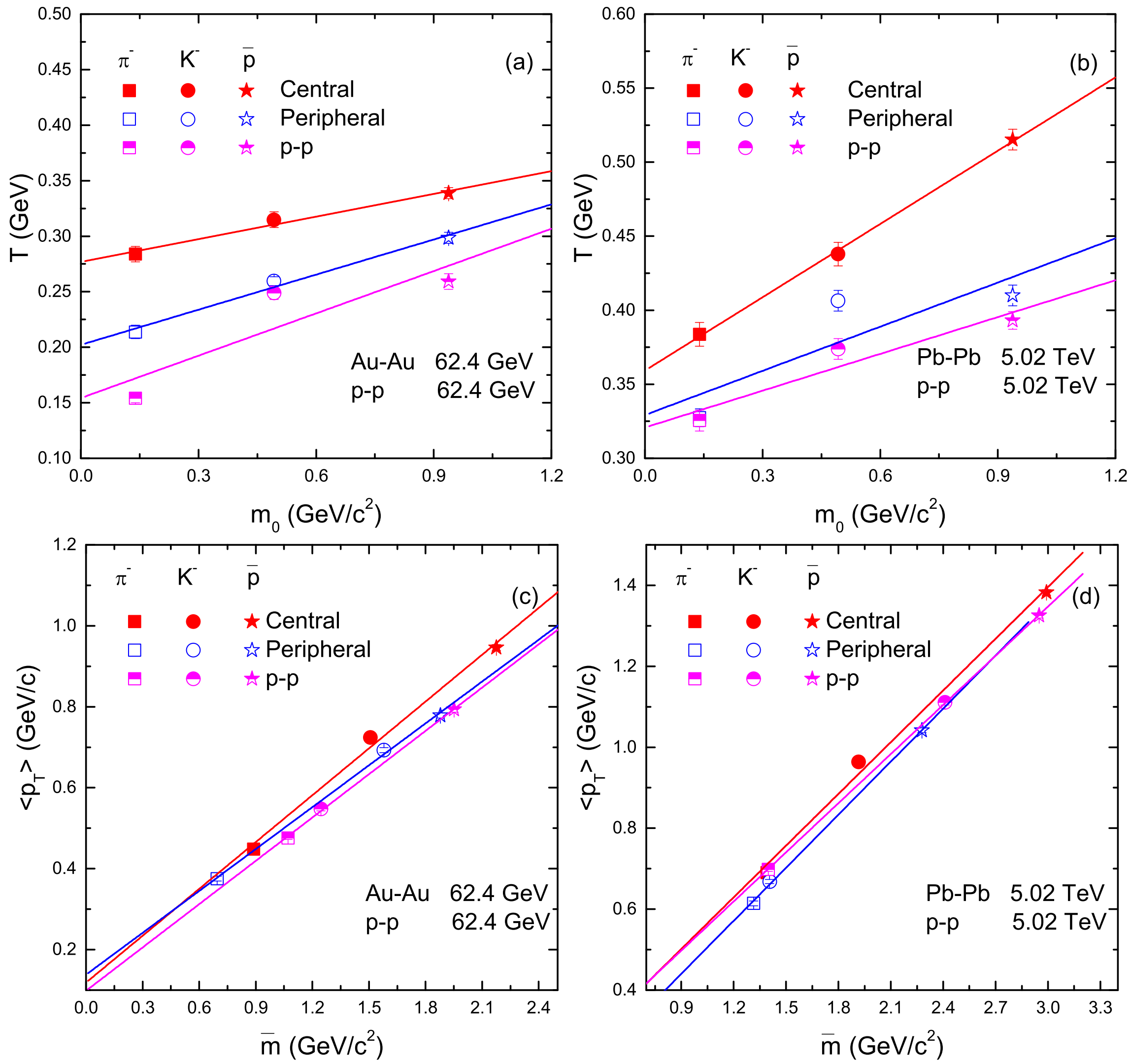

Fig. 4 (Color online) Dependences of **a**, **b** T on m_0 and **c**, **d** $\langle p_T \rangle$ on $\overline{m}$ for negatively charged particles produced in **a**, **c** central and peripheral Au–Au collisions as well as pp collisions at 62.4 GeV, and in **b**, **d** central and peripheral Pb–Pb collisions as well as pp collisions at 5.02 TeV. The filled, empty, and half-filled symbols represent the parameter values from central AA, peripheral AA, and pp collisions, respectively. The lines are linear fits for the parameter values

Table 2 Values of slopes, intercepts, and χ^2 in the linear relations $T = am_0 + T_0$ and $\langle p_T \rangle = \beta_T \overline{m} + b$, where T, m_0 ($\overline{m}$), and $\langle p_T \rangle$ are in the units of GeV, GeV/c^2 and GeV/c, respectively

Figure	Relation	$\sqrt{s_{NN}}$ ($\sqrt{s}$)	Collisions	a (c^2), β_T (c)	T_0 (GeV), b (GeV/c)	χ^2
Figure 4a	$T - m_0$	62.4 GeV	Central Au–Au	0.0679 ± 0.006	0.2769 ± 0.006	1
			Peripheral Au–Au	0.1054 ± 0.005	0.2022 ± 0.004	1
			pp	0.1270 ± 0.005	0.1543 ± 0.006	40
Figure 4b	$T - m_0$	5.02 TeV	Central Pb–Pb	0.1650 ± 0.004	0.3593 ± 0.006	1
			Peripheral Pb–Pb	0.0994 ± 0.005	0.3293 ± 0.005	31
			pp	0.0829 ± 0.005	0.3208 ± 0.006	6
Figure 4c	$\langle p_T \rangle - \overline{m}$	62.4 GeV	Central Au–Au	0.3857 ± 0.004	0.1186 ± 0.006	23
			Peripheral Au–Au	0.3449 ± 0.006	0.1381 ± 0.004	5
			pp	0.3567 ± 0.006	0.0983 ± 0.005	1
Figure 4d	$\langle p_T \rangle - \overline{m}$	5.02 TeV	Central Pb–Pb	0.4260 ± 0.006	0.1178 ± 0.005	37
			Peripheral Pb–Pb	0.4371 ± 0.005	0.0465 ± 0.004	2
			pp	0.4048 ± 0.006	0.1331 ± 0.005	1

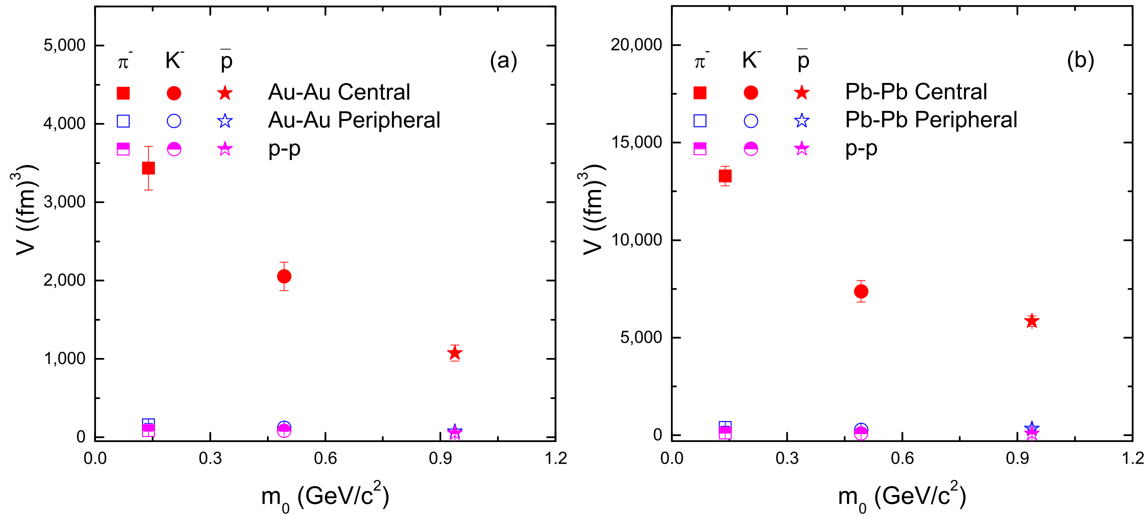

Fig. 5 (Color online) Dependences of V on m_0 for negatively charged particles produced in **a** central and peripheral Au–Au collisions as well as pp collisions at 62.4 GeV, and in **b** central and peripheral Pb–Pb collisions as well as pp collisions at 5.02 TeV. The filled, empty, and half-filled symbols represent the parameter values from central AA, peripheral AA, and pp collisions, respectively

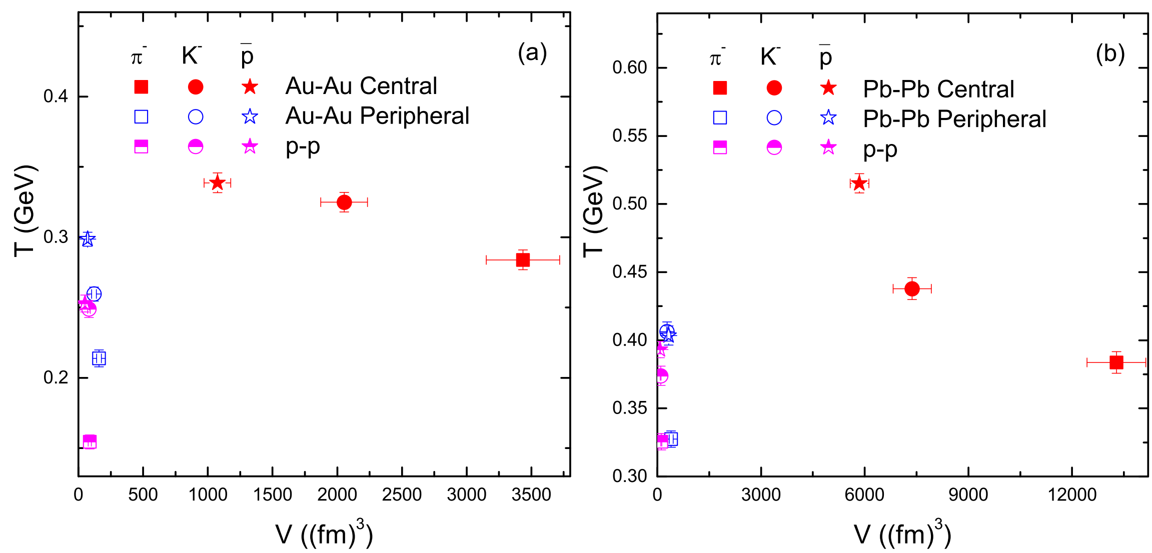

Fig. 6 (Color online) Same as Fig. 5, but showing the dependences of T on V

conclusion for the mass dependence. However, if we first fit π^- and K^- and then include $\bar{p}$, we can see that T_0 (β_T) increases (decreases slightly) with increasing the mass. Thus, we observe the mass dependence or differential kinetic freeze-out.

It should be noted that although Fig. 4 also shows the enhancement of T when m_0 increases, this has been observed in many experiments and was reported for the first time by NA44 Collaboration [45] as evidence of the flow. This result was from a fit of p_T to a thermal model for π^-, K^-, and $\bar{p}$. This indicates that the use of the two-component source model is unnecessary to observe the enhancement of T when m_0 increases. Although one can arrive at the same conclusion using a single-component source model, the two-component source model can describe well the p_T spectra. In addition, including the hard component, the model can describe better the p_T spectra.

The mass dependence of T (T_0) and β_T exists because it reflects the mass dependence of $\langle p_T \rangle$. We do not think that the mass dependence of T (T_0) and β_T is a model dependence, though the values of T (T_0) and β_T themselves are model dependent. In our fittings, we have used the same p_T range for π^-, K^-, and $\bar{p}$, while in the blast-wave fitting, different p_T ranges were used for the three types of particles [2]. The treatment by the latter increases the flexibility in the selection of parameters.

Figure 5a shows the dependences of kinetic freeze-out volume V on rest mass m_0 for production of negatively charged particles in central and peripheral Au–Au collisions at $\sqrt{s_{NN}} = 62.4$ GeV as well as in pp collisions at $\sqrt{s} = 62.4$ GeV, while Fig. 5b shows the dependences of V on m_0 for negatively charged particles produced in central and peripheral Pb–Pb collisions at $\sqrt{s_{NN}} = 5.02$ TeV as well as in pp collisions at $\sqrt{s} = 5.02$ TeV. The filled, empty, and half-filled symbols represent the central AA, peripheral AA, and pp collisions, respectively, and they represent the results weighted by different contribution fractions (volumes) in two components listed in Table 1.

It can be seen from Fig. 5 that V in central AA collisions for all the particles are larger than those in peripheral AA collisions, which shows more participant nucleons and larger expansion in central AA collisions as compared to that in the peripheral AA collisions. Meanwhile, V in pp collisions is less than that in peripheral AA collisions of the same $\sqrt{s_{NN}}$ ($\sqrt{s}$), which is caused by fewer participant nucleons (less multiplicity) in pp collisions. It is also observed that V decreases with an increase of m_0. This leads to a volume-dependent or differential freeze-out scenario and indicates different freeze-out surfaces for different particles, depending on their masses that show early freeze-out of heavier particles as compared to the lighter particles [10, 11].

Figure 6 shows the dependences of T on V for the production of negatively charged particles in (a) central and peripheral Au–Au collisions as well as in pp collisions at 62.4 GeV, and in (b) central and peripheral Pb–Pb collisions as well as in pp collisions at 5.02 TeV. The filled, empty, and half-filled symbols represent central AA, peripheral AA, and pp collisions, respectively. One can see that T decreases with the increase in V in the central and peripheral AA and pp collisions. This result is natural due to the fact that a large V corresponds to a long kinetic freeze-out time and then a cool system and a low T.

As we have not done any systematic analysis of the mass dependence of T_0 (β_T) in the present work, we shall not study the relation between T_0 (β_T) and V, though we can still predict the trend. As a supplement, our recent work [46] reported the mass dependence (slight dependence) of T_0 (β_T) using the same method as used in the present work, but using the Tsallis distribution as the "thermometer." We understand that with increasing m_0 (decreasing V), T_0 would increase naturally, and β_T would decrease slightly.

From Figs. 4, 5 and 6, one can see that T, T_0, β_T, and V obtained from collisions at the LHC are larger than those obtained from the collisions at the RHIC. This is expected due to more violent collisions happening at higher energy. However, from the RHIC to LHC, the increase in the collision energy is considerably large, and the increases in T, T_0, β_T, and V are relatively small. This reflects the penetrability of the projectiles in the transparent target. In addition, pions correspond to a larger V than protons in some cases. This is caused by the fact that pions have larger β_T and thus reach larger distance than protons due to the smaller m_0 in the case of the former at similar momenta for pions and protons at the kinetic freeze-out. This hypothesis is true because V is a reflection of multiplicity, and the experimental results indicate an enhancement in the hadron source with the multiplicity.

The result that pions correspond to a much larger V than protons indicates that the protons cease to interact while pions are still interacting. One may think that pions and protons stop interacting in different V, where large V corresponds to long interaction time. As protons have larger m_0 than pions, protons are left behind as the system evolved from the origin of collisions to the radial direction, which is the behavior of hydrodynamics [47]. This results in the volume-dependent freeze-out scenario that shows the early freeze-out of heavier particles as compared to the lighter particles [10, 11]. Thus, pions correspond to larger interacting volumes than protons, at the kinetic freeze-out stage.

To further study the dependences of T and V on centrality and collisions energy, Table 3 compiles the values of average T ($\langle T\rangle$) and average V ($\langle V\rangle$) for different types of collisions at the RHIC and LHC. These averages are obtained by different particle weights due to different contribution fractions (V) of π^-, K^-, and $\bar{p}$. One can see that $\langle T\rangle$ and $\langle V\rangle$ at the LHC are larger than those at the

Table 3 Values of $\langle T\rangle$ and $\langle V\rangle$ for different types of collisions at the RHIC and LHC

Figure	$\sqrt{s_{NN}}$ ($\sqrt{s}$)	Collisions	$\langle T\rangle$ (GeV)	$\langle V\rangle$ (fm^3)
Figure 1a	62.4 GeV	Central Au–Au	0.303 ± 0.007	2610 ± 218
Figure 1b		Peripheral Au–Au	0.247 ± 0.007	130 ± 17
Figure 3a		pp	0.214 ± 0.006	77 ± 10
Figure 2a	5.02 TeV	Central Pb–Pb	0.478 ± 0.009	10002 ± 658
Figure 2b		Peripheral Pb–Pb	0.374 ± 0.008	344 ± 54
Figure 3b		pp	0.360 ± 0.006	100 ± 13

The average values are obtained by different weights due to different contribution fractions (V) of π^-, K^-, and $\bar{p}$

RHIC. Generally, the value of T lies between T_{ch} and T_0. In particular, T_{ch} in central AA collisions is approximately 160 MeV, and T_0 in central AA collisions is less than 130 MeV [26, 27, 48, 49]. However, the values of $\langle T \rangle$ in Table 3 are larger because of Eq. (4) was used. Equation (4) contains the contributions of both thermal motion and flow effect, which can be regarded as a different "thermometer" from the literature [26, 27, 48–50] and results in different T that is beyond the general range of $[T_{ch}, T_0]$.

Even for T_0 (the intercept in Table 2 for Fig. 4a, b) obtained from $T = am_0 + T_0$, one can see the larger values. This is caused by the use of a different "thermometers." If other fitting functions are used [25–29], the obtained T_0 will be larger or smaller depending on the fitting function. For β_T (the slope in Table 2 for Fig. 4c, d) obtained from $\langle p_T \rangle = \beta_T \overline{m} + b$, one can see different values in the case of other methods ("thermometers") [20–22, 24]. Anyhow, the relative sizes of T_0 (β_T) obtained from the present work for different events centralities, system sizes, and collision energies are useful and significant. Generally, $T_0 \leq T_{ch}$. However, because of different "thermometers," we cannot simply compare the two temperatures.

Although the absolute values of T (T_0) and β_T obtained in the present work are possibly inconsistent with other results, the relative values are worth considering. Similar is true for V. The present work shows that V in central and peripheral Pb–Pb and pp collisions at 5.02 TeV is also larger than that in central and peripheral Au–Au and pp collisions at 62.4 GeV. This shows a strong dependence of the parameters on the collision energy. Furthermore, V in central and peripheral Pb–Pb collisions is larger than that in central and peripheral Au–Au collisions also shows parameter dependence on the size of the system, though this dependence can be neglected due to a small difference in the size. The dependence of collision energy and system size is not discussed here in detail because of the unavailability of a wide range of analyses but it can be focused in future work.

3.3 Further discussion

Before the summary and conclusions, we would like to point out that the method that the related parameters can be extracted from the p_T spectra of the identified particles seems approximately effective in high energy collisions. At high energy (dozens of GeV and above), the particle-dependent chemical potential μ is less than several MeV, which affects the parameters less. Equations (1)–(4) can be used in the present work. We believe that our result on the source volume for pp collisions being larger than that (~ 34 fm^3) by the femtoscopy with two-pion Bose–Einstein correlations [51] is caused by the use of different methods.

At intermediate and low energies, the method used here seems unsuitable due to the fact that the particle dependent μ at kinetic freeze-out is large and unavailable. In general, the particles of different species develop μ differently from chemical freeze-out to kinetic freeze-out. This seems to result in more difficulty in applying Eqs. (1)–(4) at intermediate and low energies. μ has less influence on the extraction of source volume due to its less influence on the data normalization or multiplicity.

As we know, the source volume is proportional to the data normalization or multiplicity. Although we can obtain the normalization or multiplicity from a model, the obtained value is almost independent of the model. In other words, the normalization or multiplicity reflects the data, but not the model itself. Different methods do not affect the source volume considerably due to the normalization or multiplicity being one of the main factors, if not the only one. In the case of using a significant μ, neglecting the radial flow, and using T, there is no considerable influence on the normalization or multiplicity, then on the source volume.

In addition, although we use the method of linear relation to obtain T_0 and β_T in the present work, we used the blast-wave model [20, 21, 24, 25] to obtain the two parameters in our previous works [22, 43, 44]. Besides, we could add indirectly the flow velocity in the treatment of standard distribution [52]. Because of different "thermometers" (fit functions) being used in different methods, the "measured" temperatures have different values, though the same trend can be observed in the same or similar collisions. The results obtained from different "thermometers" can be checked with each other.

In particular, we obtained a higher temperature, though it is also the kinetic freeze-out temperature and describes the excitation degree of emission source at the kinetic freeze-out stage. We cannot compare the T_0 obtained in the present work with T_{ch} used in the literature directly due to different "thermometers." We found that the present work gives the same trend for main parameters when we compare them with our previous works [22, 43, 44], which used the blast-wave model [20, 21, 24, 25]. It may be possible that the relative size of the main parameters in central and peripheral collisions as well as in AA and pp collisions will be the same if we use the standard distribution and the blast-wave model.

It should be pointed out that although we have studied some parameters at the stage of kinetic freeze-out, the parameters at the stage of chemical freeze-out are lacking in this study. In fact, the parameters at the stage of chemical freeze-out are more important [53–58] to map the phase diagram in which μ is an essential factor. Both the

T_{ch} and μ are the most important parameters at the chemical freeze-out stage. In the extensive statistics and/or axiomatic/generic non-extensive statistics [53–55], one may discuss the chemical and/or kinetic freeze-out parameters systematically.

Reference [56] has tried to advocate a new parametrization procedure rather than the standard χ^2 procedure with yields. The authors constructed the mean value of conserved charges and have utilized their ratios to extract T_{ch} and μ. Reference [57] evaluated systematic error arising due to the chosen set of particle ratios and constraints. A centrality dependent study for the chemical freeze-out parameters [58] could be obtained. Meanwhile, with the help of the single-freeze-out model in the chemical equilibrium framework [59, 60], reference [61] studied the centrality dependence of freeze-out temperature fluctuations in high energy *AA* collisions.

We are very interested to do a uniform study on the chemical and kinetic freeze-out parameters in the future. Meanwhile, the distribution characteristics of various particles produced in high energy collisions are very abundant [62–65], and the methods of modeling analysis are multiple. We hope to study the spectra of multiplicities, transverse energies, and transverse momenta of various particles produced in different collisions by a uniform method, in which the probability density function contributed by each participant parton is considered carefully.

4 Summary and conclusions

We summarize here our main observations and conclusions

(a) Main parameters extracted from the transverse momentum spectra of identified particles produced in central and peripheral Au–Au collisions at 62.4 GeV and Pb–Pb collisions at 5.02 TeV were studied. Furthermore, the same analysis was done for *pp* collisions at both RHIC and LHC energies. The two-component standard distribution was used, which included both the very soft and soft excitation processes. The effective temperature, kinetic freeze-out temperature, transverse flow velocity, and kinetic freeze-out volume were found to be larger in central collisions as compared to that in the peripheral collisions, which shows higher excitation and larger expansion in central collisions.

(b) Effective temperatures in central and peripheral Au–Au (Pb–Pb) collisions at the RHIC (LHC) increased with increasing the particle mass, which showed a mass-dependent differential kinetic freeze-out scenario at RHIC and LHC energies. The kinetic freeze-out temperature is also expected to increase with increasing the particle's mass. The kinetic freeze-out volume decreased with the increase of particle mass that showed different values for different particles and indicated a volume-dependent differential kinetic freeze-out scenario. The transverse flow velocity is expected to decrease slightly with the increase of particle mass.

(c) Effective (kinetic freeze-out) temperatures in peripheral Au–Au and *pp* collisions at 62.4 GeV as well as in peripheral Pb–Pb and *pp* collisions at 5.02 TeV were, respectively, similar and had a similar trend, which showed similar thermodynamic nature of the parameters in peripheral *AA* and *pp* collisions at the same center-of-mass energy (per nucleon pair). Effective (kinetic) freeze-out) temperatures in both central and peripheral *AA* and *pp* collisions decreased with an increase in the kinetic freeze-out volume. The transverse flow velocity is expected to increase slightly with the increase in the kinetic freeze-out volume in the considered energy range.

(d) Effective (kinetic freeze-out) temperature, transverse flow velocity, and kinetic freeze-out volume in central and peripheral *AA* and *pp* collisions at the LHC were larger than those at the RHIC, which showed their dependence on collision energy. Also, central (peripheral) Pb–Pb collisions rendered slightly larger effective (kinetic freeze-out) temperature, transverse flow velocity, and kinetic freeze-out volume than central (peripheral) Au–Au collisions. This showed the dependence of the parameters on the size of the system, which could be neglected for Pb–Pb and Au–Au collisions due to their small difference in the size.

References

1. N. Xu, (for the STAR Collaboration), An overview of STAR experimental results. Nucl. Phys. A **931**, 1 (2014). https://doi.org/10.1016/j.nuclphysa.2014.10.022
2. S. Chatterjee, S. Das, L. Kumar et al., Freeze-out parameters in heavy-ion collisions at AGS, SPS, RHIC, and LHC energies. Adv. High Energy Phys. **2015**, 349013 (2015). https://doi.org/10.1155/2015/349013
3. S. Chatterjee, B. Mohanty, R. Singh, Freezeout hypersurface at energies available at the CERN Large Hadron Collider from particle spectra: flavor and centrality dependence. Phys. Rev. C **92**, 024917 (2015). https://doi.org/10.1103/PhysRevC.92.024917
4. S. Chatterjee, B. Mohanty, Production of light nuclei in heavyion collisions within a multiple-freezeout scenario. Phys. Rev. C **90**, 034908 (2014). https://doi.org/10.1103/PhysRevC.90.034908
5. S.S. Räsänen, (for the ALICE Collaboration), ALICE overview. EPJ Web Conf. **126**, 02026 (2016). https://doi.org/10.1051/epjconf/201612602026

6. X.-F. Luo, N. Xu, Search for the QCD critical point with fluctuations of conserved quantities in relativistic heavy-ion collisions at RHIC: an overview. Nucl. Sci. Tech. **28**, 112 (2017). https://doi.org/10.1007/s41365-017-0257-0
7. H.C. Song, Y. Zhou, K. Gajdošová, Collective flow and hydrodynamics in large and small systems at the LHC. Nucl. Sci. Tech. **28**, 99 (2017). https://doi.org/10.1007/s41365-017-0245-4
8. G. Bertsch, P.J. Siemens, Nuclear fragmentation. Phys. Lett. B **126**, 9 (1983). https://doi.org/10.1016/0370-2693(83)90004-7
9. L.G. Moretto, G.J. Wozniak, Multifragmentation in heavy ion processes. Annu. Rev. Nucl. Part. Sci. **43**, 379 (1993). https://doi.org/10.1146/annurev.ns.43.120193.002115
10. D. Thakur, S. Tripathy, P. Garg et al., Indication of differential kinetic freeze-out at the RHIC and LHC energies. Acta Phys. Pol. B Proc. Suppl. **9**, 329 (2016). https://www.actaphys.uj.edu.pl/S/9/2/329/pdf
11. D. Thakur, S. Tripathy, P. Garg et al., Indication of a differential freeze-out in proton-proton and heavy-ion collisions at the RHIC and LHC energies. Adv. High Energy Phys. **2016**, 4149352 (2016). https://doi.org/10.1155/2016/4149352
12. D.H.E. Gross, Microcanonical thermodynamics and statistical fragmentation of dissipative systems: the topological structure of the N-body phase space. Phys. Rep. **279**, 119 (1997). https://doi.org/10.1016/S0370-1573(96)00024-5
13. B. Borderie, Dynamics and thermodynamics of the liquid–gas phase transition in hot nuclei studied with the INDRA array. J. Phys. G **28**, R217 (2002). https://doi.org/10.1088/0954-3899/28/8/201
14. M. D'Agostino, F. Gulminelli, P. Chomaz et al., Negative heat capacity in the critical region of nuclear fragmentation: an experimental evidence of the liquid–gas phase transition. Phys. Lett. B **473**, 219 (2000). https://doi.org/10.1016/S0370-2693(99)01486-0
15. M. D'Agostino, R. Bougault, F. Gulminelli et al., On the reliability of negative heat capacity measurements. Nucl. Phys. A **699**, 795 (2002). https://doi.org/10.1016/S0375-9474(01)01287-8
16. P. Chomaz, V. Duflot, F. Gulminelli, Caloric curves and energy fluctuations in the microcanonical liquid–gas phase transition. Phys. Rev. Lett. **85**, 3587 (2000). https://doi.org/10.1103/PhysRevLett.85.3587
17. R. Hagedorn, Multiplicities, p_T distributions and the expected hadron → quark–gluon phase transition. Riv. Nuovo Cimento **6**(10), 1 (1983). https://doi.org/10.1007/BF02740917
18. J. Cleymans, D. Worku, Relativistic thermodynamics: transverse momentum distributions in high-energy physics. Eur. Phys. J. A **48**, 160 (2012). https://doi.org/10.1140/epja/i2012-12160-0
19. H. Zheng, L.L. Zhu, Comparing the Tsallis distribution with and without thermodynamical description in $p+p$ collisions. Adv. High Energy Phys. **2016**, 9632126 (2016). https://doi.org/10.1155/2016/9632126
20. Z.B. Tang, Y.C. Xu, L.J. Ruan et al., Spectra and radial flow in relativistic heavy ion collisions with Tsallis statistics in a blast-wave description. Phys. Rev. C **79**, 051901(R) (2009). https://doi.org/10.1103/PhysRevC.79.051901
21. E. Schnedermann, J. Sollfrank, U.W. Heinz, Thermal phenomenology of hadrons from the 200 A GeV S + S collisions. Phys. Rev. C **48**, 2462 (1993). https://doi.org/10.1103/PhysRevC.48.2462
22. H.-L. Lao, F.-H. Liu, B.-C. Li et al., Kinetic freeze-out temperatures in central and peripheral collisions: which one is larger? Nucl. Sci. Tech. **29**, 82 (2018). https://doi.org/10.1007/s41365-018-0425-x
23. H.-L. Lao, F.-H. Liu, B.-C. Li et al., Examining the model dependence of the determination of kinetic freeze-out temperature and transverse flow velocity in small collision system. Nucl. Sci. Tech. **29**, 164 (2018). https://doi.org/10.1007/s41365-018-0504-z
24. B.I. Abelev et al., (STAR Collaboration), Systematic measurements of identified particle spectra in pp, d + Au, and Au + Au collisions at the STAR detector. Phys. Rev. C **79**, 034909 (2009). https://doi.org/10.1103/PhysRevC.79.034909
25. B.I. Abelev et al., (STAR Collaboration), Identified particle production, azimuthal anisotropy, and interferometry measurements in Au + Au collisions at $\sqrt{s_{NN}} = 9.2$ GeV. Phys. Rev. C **81**, 024911 (2010). https://doi.org/10.1103/PhysRevC.81.024911
26. J. Cleymans, H. Oeschler, K. Redlich et al., Comparison of chemical freeze-out criteria in heavy-ion collisions. Phys. Rev. C **73**, 034905 (2006). https://doi.org/10.1103/PhysRevC.73.034905
27. A. Andronic, P. Braun-Munzinger, J. Stachel, Hadron production in central nucleus–nucleus collisions at chemical freeze-out. Nucl. Phys. A **772**, 167 (2006). https://doi.org/10.1016/j.nuclphysa.2006.03.012
28. S. Uddin, J.S. Ahmad, W. Bashir et al., A unified approach towards describing rapidity and transverse momentum distributions in a thermal freeze-out model. J. Phys. G **39**, 015012 (2012). https://doi.org/10.1088/0954-3899/39/1/015012
29. R.P. Adak, S. Das, S.K. Ghosh et al., Centrality dependence of chemical freeze-out parameters from net-proton and net-charge fluctuations using a hadron resonance gas model. Phys. Rev. C **96**, 014902 (2017). https://doi.org/10.1103/PhysRevC.96.014902
30. R. Odorico, Does a transverse energy trigger actually trigger on large-p_T jets? Phys. Lett. B **118**, 151 (1982). https://doi.org/10.1016/0370-2693(82)90620-7
31. K. Aamodt et al., (ALICE Collaboration), Transverse momentum spectra of charged particles in proton–proton collisions at $\sqrt{s} =$ 900 GeV with ALICE at the LHC. Phys. Lett. B **693**, 53 (2010). https://doi.org/10.1016/j.physletb.2010.08.026
32. T. Mizoguchi, M. Biyajima, N. Suzuki, Analyses of whole transverse momentum distributions in $p\bar{p}$ and pp collisions by using a modified version of Hagedorn's formula. Int. J. Mod. Phys. A **32**, 1750057 (2017). https://doi.org/10.1142/S0217751X17500579
33. H.-L. Lao, Y.-Q. Gao, F.-H. Liu, Light particle and quark chemical potentials from negatively to positively charged particle yield ratios corrected by removing strong and weak decays. Adv. High Energy Phys. **2020**, 5064737 (2020). https://doi.org/10.1155/2020/5064737
34. M. Shao, (for the STAR Collaboration), Pion, kaon and (anti-)proton production in Au + Au collisions at $\sqrt{s_{NN}} = 62.4$ GeV. J. Phys. G **31**, S85 (2005). https://doi.org/10.1088/0954-3899/31/4/011
35. Y.C. Morales, N. Hussain, N. Jacazio et al., Production of pions, kaons and protons in pp and Pb–Pb collisions at $\sqrt{s} = 5.02$ TeV. CERN Preprint (ALICE Analysis Note 2016) ALICE-ANA-2016-xxx (July 12, 2017). http://alice-notes.web.cern.ch/, July 24, 2019
36. S. Acharya et al., (ALICE Collaboration), Production of charged pions, kaons, and (anti-)protons in Pb–Pb and inelastic pp collisions at $\sqrt{s_{NN}} = 5.02$ TeV. Phys. Rev. C **101**, 044907 (2020). https://doi.org/10.1103/PhysRevC.101.044907
37. A. Adare et al., (PHENIX Collaboration), Identified charged hadron production in $p+p$ collisions at $\sqrt{s} = 200$ and 62.4 GeV. Phys. Rev. C **83**, 064903 (2011). https://doi.org/10.1103/PhysRevC.83.064903
38. P.-P. Yang, M.-Y. Duan, F.-H. Liu et al., Multiparticle production and initial quasitemperature from proton-induced carbon collisions at $p_{Lab} = 31$ GeV/c. Adv. High Energy Phys. **2020**, 9542196 (2020). https://doi.org/10.1155/2020/9542196
39. S. Takeuchi, K. Murase, T. Hirano et al., Effects of hadronic rescattering on multistrange hadrons in high-energy nuclear

collisions. Phys. Rev. C **92**, 044907 (2015). https://doi.org/10.1103/PhysRevC.92.044907

40. H. Heiselberg, A.-M. Levy, Elliptic flow and Hanbury–Brown–Twiss correlations in noncentral nuclear collisions. Phys. Rev. C **59**, 2716 (1999). https://doi.org/10.1103/PhysRevC.59.2716
41. H.-R. Wei, F.-H. Liu, R.A. Lacey, Kinetic freeze-out temperature and flow velocity extracted from transverse momentum spectra of final-state light flavor particles produced in collisions at RHIC and LHC. Eur. Phys. J. A **52**, 102 (2016). https://doi.org/10.1140/epja/i2016-16102-6
42. H.-R. Wei, F.-H. Liu, R.A. Lacey, Disentangling random thermal motion of particles and collective expansion of source from transverse momentum spectra in high energy collisions. J. Phys. G **43**, 125102 (2016). https://doi.org/10.1088/0954-3899/43/12/125102
43. M. Waqas, F.-H. Liu, S. Fakhraddin et al., Possible scenarios for single, double, or multiple kinetic freeze-out in high-energy collisions. Indian J. Phys. **93**, 1329 (2019). https://doi.org/10.1007/s12648-019-01396-9
44. M. Waqas, F.-H. Liu, Centrality dependence of kinetic freeze-out temperature and transverse flow velocity in high energy nuclear collisions. Indian J. Phys. arXiv:1806.05863 [hep-ph] (2018). **(Submitted)**
45. I.G. Bearden et al., (NA44 Collaboration), Collective expansion in high energy heavy ion collisions. Phys. Rev. Lett. **78**, 2080 (1997). https://doi.org/10.1103/PhysRevLett.78.2080
46. H.-L. Lao, H.-R. Wei, F.-H. Liu et al., An evidence of mass-dependent differential kinetic freeze-out scenario observed in Pb–Pb collisions at 2.76 TeV. Eur. Phys. J. A **52**, 203 (2016). https://doi.org/10.1140/epja/i2016-16203-2
47. R. Sahoo, Possible formation of QGP-droplets in proton–proton collisions at the CERN Large Hadron Collider. AAPPS Bull. **29**(4), 16 (2019). https://doi.org/10.22661/AAPPSBL.2019.29.4.16
48. A. Andronic, P. Braun-Munzinger, J. Stachel, Thermal hadron production in relativistic nuclear collisions. Acta Phys. Pol. B **40**, 1005 (2009). https://www.actaphys.uj.edu.pl/R/40/4/1005/pdf
49. A. Andronic, P. Braun-Munzinger, J. Stachel, The horn, the hadron mass spectrum and the QCD phase diagram—the statistical model of hadron production in central nucleus–nucleus collisions. Nucl. Phys. A **834**, 237c (2010). https://doi.org/10.1016/j.nuclphysa.2009.12.048
50. F.G. Gardim, G. Giacalone, M. Luzum et al., Thermodynamics of hot strong-interaction matter from ultrarelativistic nuclear collisions. Nature Phys. **16**, 615 (2020). https://doi.org/10.1038/s41567-020-0846-4
51. K. Aamodt et al., (ALICE Collaboration), Femtoscopy of *pp* collisions at $\sqrt{s} = 0.9$ and 7 TeV at the LHC with two-pion Bose–Einstein correlations. Phys. Rev. D **84**, 112004 (2011). https://doi.org/10.1103/PhysRevD.84.112004
52. F.-H. Liu, H.-L. Lao, Blast-wave revision of the multisource thermal model in nucleus–nucleus collisions. Indian J. Phys. **90**, 1077 (2016). https://doi.org/10.1007/s12648-016-0846-5
53. A.N. Tawflk, H. Yassin, E.R. Abo Elyazeed, Extensive/nonextensive statistics for p_T distributions of various charged particles produced in p + p and A + A collisions in a wide range of energies. arXiv:1905.12756 [hep-ph] (2019)
54. A.N. Tawflk, Axiomatic nonextensive statistics at NICA energies. Eur. Phys. J. A **52**, 253 (2016). https://doi.org/10.1140/epja/i2016-16253-4
55. A.N. Tawflk, H. Yassin, E.R. Abo Elyazeed, Chemical freezeout parameters within generic nonextensive statistics. Indian J. Phys. **92**, 1325 (2018). https://doi.org/10.1007/s12648-018-1216-2
56. S. Bhattacharyya, D. Biswas, S.K. Ghosh et al., Novel scheme for parametrizing the chemical freeze-out surface in heavy ion collision experiments. Phys. Rev. D **100**, 054037 (2019). https://doi.org/10.1103/PhysRevD.100.054037
57. S. Bhattacharyya, D. Biswas, S.K. Ghosh et al., Systematics of chemical freeze-out parameters in heavy-ion collision experiments. Phys. Rev. D **101**, 054002 (2020). https://doi.org/10.1103/PhysRevD.101.054002
58. D. Biswas, Centrality dependence of chemical freeze-out parameters and strangeness equilibration in RHIC and LHC. arXiv:2003.10425 [hep-ph] (2020)
59. D. Prorok, Single freeze-out, statistics and pion, kaon and proton production in central Pb–Pb collisions at $\sqrt{s_{NN}} = 2.76$ TeV. J. Phys. G **43**, 055101 (2016). https://doi.org/10.1088/0954-3899/43/5/055101
60. D. Prorok, Thermal freeze-out versus chemical freeze-out reexamined. Acta Phys. Pol. B **40**, 2825 (2009). https://www.actaphys.uj.edu.pl/R/40/10/2825/pdf
61. D. Prorok, Centrality dependence of freeze-out temperature fluctuations in Pb–Pb collisions at the LHC. Eur. Phys. J. A **55**, 37 (2019). https://doi.org/10.1140/epja/i2019-12709-3
62. L. Zhou, D.-Q. Fang, Effect of source size and emission time on the p–p momentum correlation function in the two-proton emission process. Nucl. Sci. Tech. **31**, 52 (2020). https://doi.org/10.1007/s41365-020-00759-w
63. H. Wang, J.-H. Chen, Y.-G. Ma et al., Charm hadron azimuthal angular correlations in Au + Au collisions at $\sqrt{s_{NN}} = 200$ GeV from part scatterings. Nucl. Sci. Tech. **30**, 185 (2019). https://doi.org/10.1007/s41365-019-0706-z
64. L.-H. Song, L.-W. Yan, Y. Liu, Constraining the colored $c\bar{c}$ energy loss from J/ψ production in p-A collisions. Nucl. Sci. Tech. **29**, 159 (2018). https://doi.org/10.1007/s41365-018-0502-1
65. S.-H. Zhang, L. Zhou, Y.-F. Zhang et al., Multiplicity dependence of charged particle, ϕ meson, and multi-strange particle productions in p + p collisions at $\sqrt{s} = 200$ GeV from PYTHIA simulation. Nucl. Sci. Tech. **29**, 136 (2018). https://doi.org/10.1007/s41365-018-0469-y